International Journal of Microwave and Wireless Technologies

cambridge.org/mrf

Novel miniaturized monolithic triplexer for dual-band GPS and Bluetooth based on LTOI

Peiran Li[1], Bin Peng[1], Zijie Wei[1], Wei Fan[1], Yuedong Wang[1], Dahao Wu[1], Lu Lv[2], Wenbo Luo[1], Yao Shuai[1], Xinqiang Pan[1] and Chuangui Wu[1]

[1]School of Integrated Circuit Science and Engineering, University of Electronic Science and Technology of China, Chengdu, China and [2]The 29th Research Institute of China Electronics Technology Group Corporation, Chengdu, China

Research Paper

Cite this article: Li P *et al*. (2026) Novel miniaturized monolithic triplexer for dual-band GPS and Bluetooth based on LTOI. *International Journal of Microwave and Wireless Technologies* **18**(4), 583–592. https://doi.org/10.1017/S175907872610347X

Received: 24 November 2025 UTC
Revised: 4 June 2026 UTC
Accepted: 10 June 2026 UTC
First published online: 10 July 2026 UTC

Keywords:
Bluetooth; dual-band GPS; monolithic; SAW; triplexer

Corresponding author: Bin Peng;
Email: bpeng@uestc.edu.cn

Abstract

With the evolution from 5G to 6G and the popularization of carrier aggregation technology, mobile terminal devices face challenges in miniaturizing multiplexers and handling concurrent signals across a wide-bandgap. This study proposes a numerical de-embedding design method. By precisely calculating and compensating for the parasitic loads, it achieves deterministic synthesis of matching networks. Based on this method, we designed and fabricated a monolithic integrated surface acoustic wave triplexer on a lithium tantalite on insulator (LTOI) substrate for dual-frequency GPS L1/L5 positioning and Bluetooth (BT) communication. To suppress a specific spurious mode on the LTOI substrate and improve the isolation, a notch inductor structure was embedded into the design. The monolithic integrated triplexer measures 2.5 mm × 2.0 mm × 0.6 mm after packaging. The insertion loss is less than 1.6 dB in both the L1 and L5 bands. In the BT band, the average loss within any 18 MHz range of the passband is below 2.5 dB. The return loss for all three channels is better than −10 dB, while the isolation between channels is maintained at ≈40 dB. The successful fabrication of this triplexer not only validates the design method but also demonstrates its potential for application in miniaturized wearable devices.

Introduction

In the transitional period from the post-5G toward 6G, the design of the radio frequency front-end (RFFE) for mobile terminals is undergoing a profound architectural revolution [1]. Currently, the widespread adoption of carrier aggregation technology, the increasing number of multiple-input multiple-output (MIMO) channels, and the congestion of noncellular communication frequency bands are reshaping the radio frequency (RF) environment [1, 2]. Therefore, achieving concurrent processing of signals across any number of frequency bands in miniaturized terminals has become a critical bottleneck. This context has greatly spurred the demand for miniaturized, high-performance multiplexers, especially in wearable devices [3–5]. Therefore, achieving both low loss and high isolation with an extremely compact size has become a challenge in the design of the next-generation RFFE.

Surface acoustic wave (SAW) filters play a vital role in modern RFFE systems through continuous innovation in materials, acoustic structure, and packaging technologies [6, 7]. Among these, lithium tantalate on insulator (LTOI) technology is increasingly demonstrating significant potential as a multiband integrated platform [8–10]. By precisely confining acoustic energy within submicron-sized piezoelectric film, LTOI can achieve resonators with a high-quality factor [11], providing an excellent physical basis for multiband integration.

For the implementation of multiplexers, traditional solutions rely on combinations of discrete components or multi-chip module packaging [12–16]. While technically feasible, these approaches suffer from drawbacks. For example, the increased number of components leads to higher system complexity, interconnect parasitic effects worsen insertion loss (IL), and miniaturization remains a challenge [17, 18]. Conversely, monolithic integration offers a promising path to improve chip yield, reduce package size, and reduce parasitic effects. However, it also imposes higher demands on substate performance and impedance matching design methodologies.

In existing multiplexer designs, the passband impedance of each channel is typically designed to be 50 Ω. For conventional duplexer designs, simple phase shifters or LC networks are widely utilized to rotate the counter-band impedance to a high-impedance region [19–26]. However, designing a triplexer with a large frequency gap remains challenging. An example is the integration of GPS L5/L1 and Bluetooth (BT), where the overall span exceeds 1.3 GHz. Under such conditions, the aforementioned design methods are no longer applicable. Additionally, the wide-bandgap will introduce issues with high-frequency spurious responses.

© The Author(s), 2026. Published by Cambridge University Press in association with The European Microwave Association.

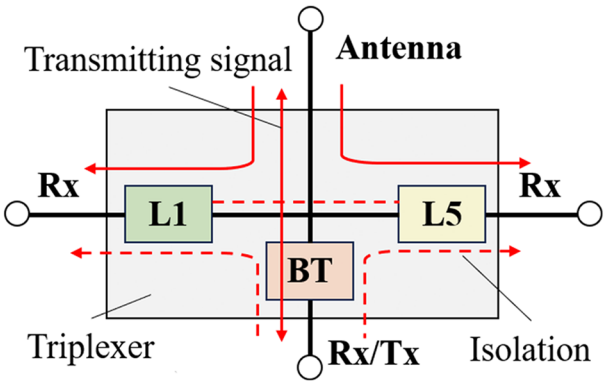


Figure 1. Basic configuration of the proposed triplexer.

Table 1. Summary of specification

Section	L5	L1	BT
Freq. (MHz)	1164–1189	1559–1606	2400–2483
IL (dB)	-1.6	-1.6	-2
RL (dB)	−10	−10	−10
OoB (dB)	−40	−40	−40
ISO (dB)	L5-BT: −40	L1-BT: −40	L1-L5: −40

ISO = isolation between two frequency bands; OoB = out-of-band rejection; RL = return loss.

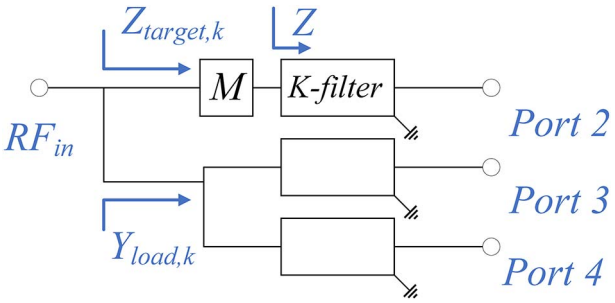


Figure 2. The schematic diagram of triplexer analytical synthesis.

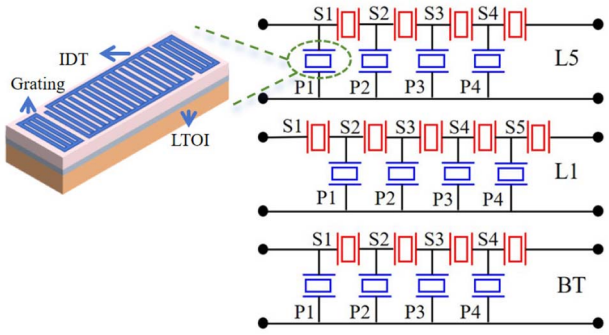


Figure 3. Circuit structure of the three individual filters.

To address these challenges, this study proposes an analytical synthesis strategy based on numerical de-embedding. This approach effectively achieves matching across a wide-bandgap of 1.3 GHz. A notch inductor structure is introduced to suppress leakage in the specific frequency band. Based on this method, we validated and realized a monolithic SAW triplexer based on LTOI substrate. This device achieves monolithic integration of dual-frequency GPS L1/L5 and BT within a compact 2.5 mm × 2 mm footprint, demonstrating significant potential for wearable applications.

Design

The proposed triplexer is designed for dual-frequency GPS L1/L5 and BT band. The basic configuration of the proposed four-port triplexer is shown in Fig. 1. As shown in Fig. 1, the L5 and L1 bands are used for dual-frequency GPS positioning signal reception, while the BT band realizes RF wireless communication transmission and reception in the RF front-end module. The dashed line in Fig. 1 represents the leakage path of the signal between the frequency bands. Good isolation between frequency bands is crucial in the device design. The frequency ranges of the L5, L1, and BT bands and other specifications of the three frequency bands are summarized in Table 1.

Analytical synthesis of matching networks

SAW filters exhibit capacitive behavior in the low-frequency regions far from the passband. This derives from the fundamental physical characteristics of SAW resonators. Utilizing this principle, we can employ numerical methods to determine the integrated matching network in triplexer design. This approach avoids the ambiguity in topology selection and simulation convergence issues often encountered in direct optimization. For triplexer design, we propose a numerical de-embedding matching method. The process can be summarized in the following four steps. The schematic diagram of the triplexer analytical synthesis is shown in Fig. 2.

Characterization of cumulative parasitic loading: For any specific channel k operating at the center frequency f_{ck}, the other $N-1$ channels are all within its stopband. Therefore, these non-operating channels introduce a significant reactive load effect at the common port. We define $Y_{load,k}$ as the cumulative load admittance. It represents the sum of the admittance of the other channels at f_{ck}:

$$Y_{load,k}(f_{ck}) = \sum_{i\neq k}^{N} Y_{in,i}(f_{ck}) = G_{para,k} + jB_{para,k} \approx jB_{para,k} \quad (1)$$

where $G_{para,k}$ and $B_{para,k}$ represent the parasitic conductance and susceptance at the frequency of channel k, respectively. When f_{ck} of channel k is in the deep rejection region (far from the passband), the conductance $G_{para,k}$ of the SAW filter can be ignored.

De-embedding complex targets: To make sure 50 Ω impedance matching at the antenna's common port, the target impedance of the matching network for channel k should be designed as a pre-distortion complex admittance $Y_{target,k}$. This admittance can effectively compensate for the parasitic load from step one. $Y_{target,k}$ can be expressed as the following equation:

$$Y_{target,k}(f_{ck}) = Y_0 - Y_{load,k}(f_{ck}) = G_0 - jB_{para,k} \quad (2)$$

where Y_0 is the characteristic admittance of 20 mS. Converted to the impedance domain, the synthetic $Z_{target,k}$ target can be expressed as:

https://doi.org/10.1017/S175907872610347X Published online by Cambridge University Press

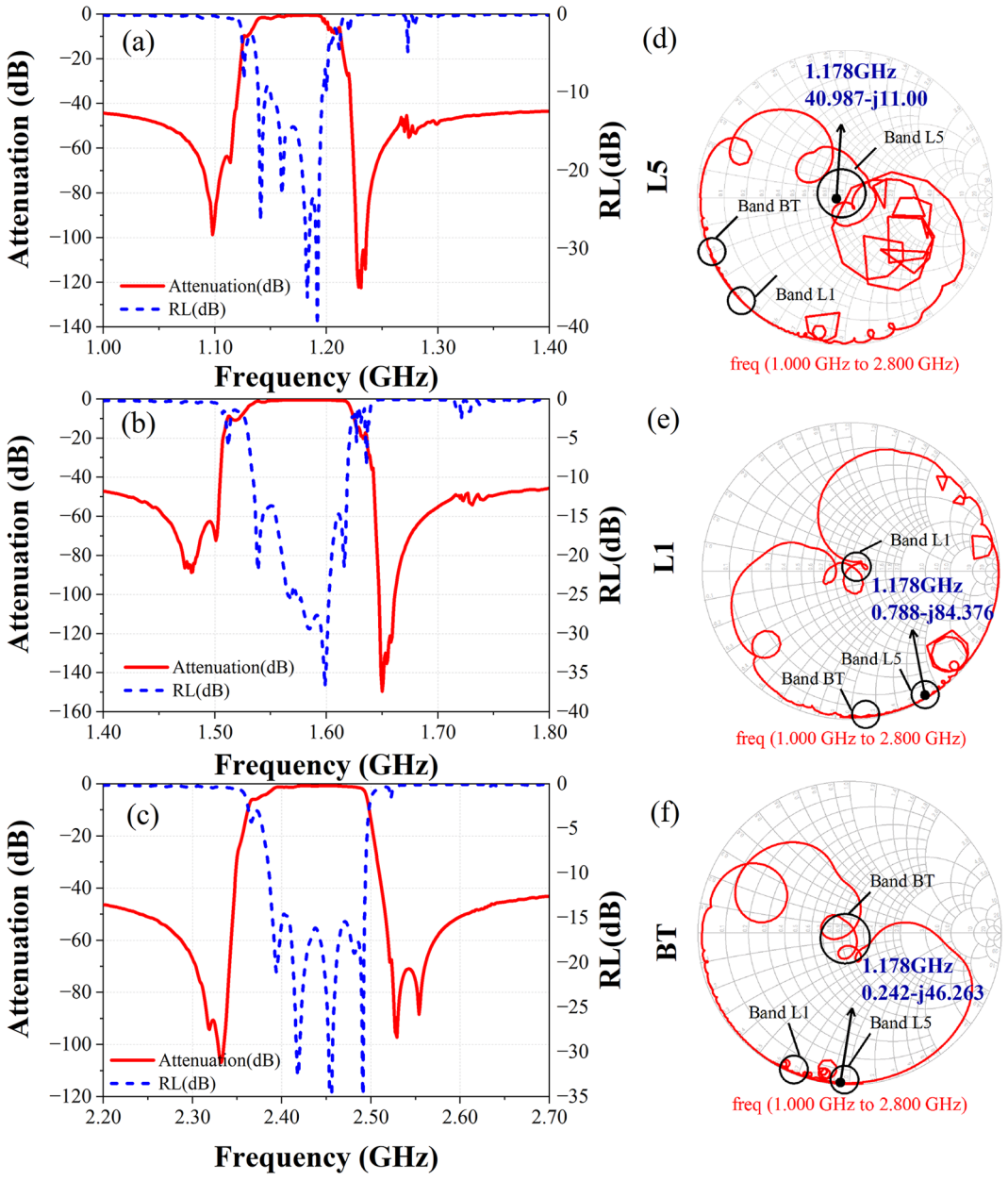


Figure 4. Simulation results of the individual filter corresponding to (a) L5, (b) L1, and (c) BT frequency band. (d)–(f) represent the S11 of the L5, L1, and BT filters in Smith chart, respectively.

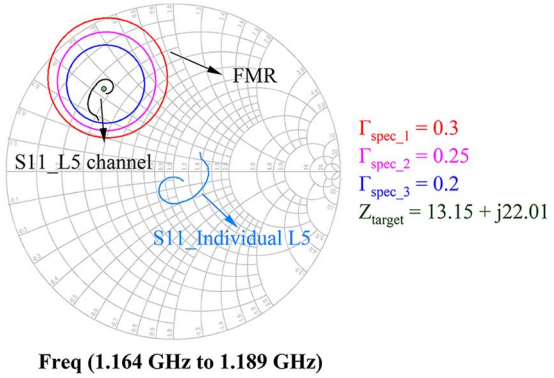


Figure 5. Smith chart with the constant reflection coefficient circles and FMR.

$$Z_{target,k} = \frac{1}{G_0 - jB_{para,k}} \tag{3}$$

Construction of feasible matching regions (FMR): The strict single-point target $Z_{target,k}$ is relaxed to a solution space that satisfies the bandwidth requirements. Therefore, we design the FMR as shown in the following equation:

$$FMR_k = \left\{ Z(f) \in \mathbb{C} \left| \left| \frac{Z(f) - Z_{target,k}}{Z(f) + Z_{target,k}} \right| \leqslant \Gamma_{spec}, \forall f \in BW_k \right. \right\}, \tag{4}$$

where Z represents complex impedance, Γ_{spec} represents the target reflection coefficient at the antenna common port, and BW_k represents the operating bandwidth of channel k. This region indicates that the antenna common port meets the system return loss (RL) requirements.

https://doi.org/10.1017/S175907872610347X Published online by Cambridge University Press

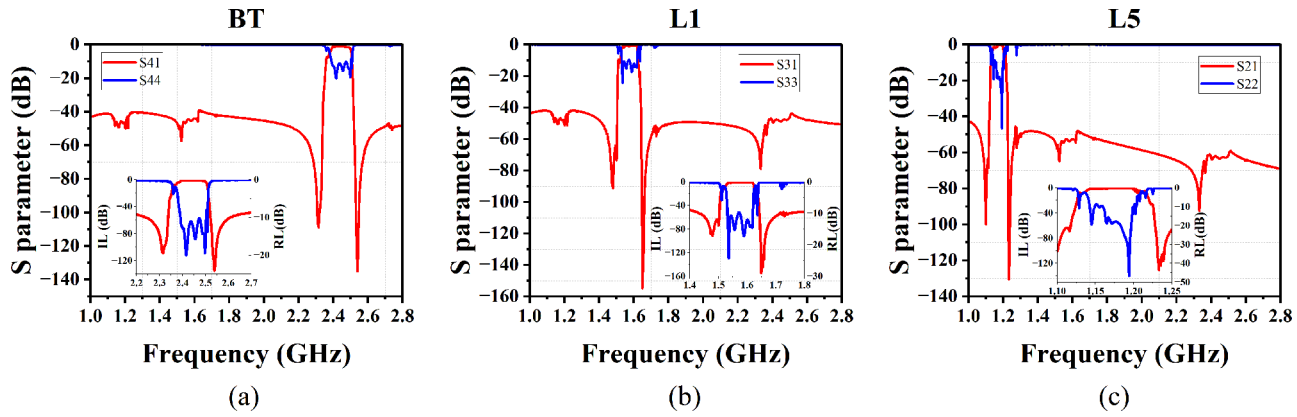


Figure 6. Simulation results of the synthesized triplexer. (a), (b) and (c) represent the performance of BT, L1, and L5, respectively.

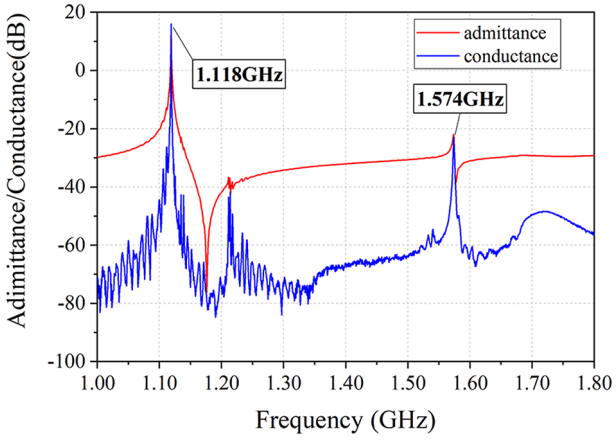


Figure 7. Measured admittance and conductance of the SAW resonator.

- **Topology and trajectory implementation**: Within the boundaries defined by FMR, one can transform the intrinsic impedance of the k-channel filter to the FMR, thus achieving the synthesis of a triplexer.

Characterization of individual filters

The circuit structure of the individual filter in the proposed triplexer is shown in Fig. 3. Each series or parallel resonator is a one-port SAW resonator based on the LTOI substrate. Ladder-type structure filters are designed in the triplexer due to their better attenuation effect on both sides of the passband and good isolation between bands. The L5 and BT filters utilize π-type ladder topology; the L1 filter utilizes a T-type topology.

The three filters shown in Fig. 3 were designed individually using the coupling-of-modes (COM) model [27]. The physical dimensions of the SAW resonators interdigital transducers (IDTs) were determined by optimizing the pitch (P), aperture (W), and number of finger pairs (N). The detailed physical parameters are listed in the Appendix. Figure 4 shows the simulation results of the three filters. From Fig. 4, it can be observed that each filter demonstrates good performance with small IL and large RL, which means that each filter is well designed.

Design of GPS L1/L5 and BT triplexer

To implement the design of the dual-frequency GPS L1/L5 and BT triplexer, we applied the numerical de-embedding synthesis method proposed in the "Analytical synthesis of matching networks" section. In this design case, given that the L5 channel is located at the lowest frequency band of the triplexer, the L1 and BT channels exhibit purely capacitive characteristics with negligible conductance in the L5 frequency range. Consequently, the L5 channel was selected as the reference channel k. Figure 4(d)–(f) presents the impedance values of each filter at the L5 center frequency (1.178 GHz). According to Eq. (1), the calculated cumulative loading admittance Y_{load} is j0.0335 S. Assuming that the system impedance is 50 Ω at the common port of the triplexer, we performed de-embedding on channel k to compensate for the parasitic loading effects from L1 and BT. Based on Eq. (2), the target admittance Y_{target} for channel k was derived as 0.02 − j0.0335 S, which corresponds to a target impedance of 13.15 + j22.01 Ω. This impedance point is defined as the ideal matching point (reflection coefficient $\Gamma = 0$) at the center frequency. Subsequently, the strict single-point target was relaxed to a solution space that satisfies the bandwidth requirements. Following this, constant reflection circles and the FMR were plotted on the Smith chart. As shown in Fig. 5, the constant reflection coefficient circles corresponding to $\Gamma = 0.2$, 0.25, and 0.3 are distributed in the inductive low-impedance region of the Smith chart. Therefore, we cascaded a matching network between the common antenna port and the L5 filter to transform the passband impedance of the L5 channel into the FMR This network consists of a series inductor and a parallel capacitor. Through this special topology configuration, the impedance trajectory of L5 was successfully rotated into the target region, thereby achieving the final matching and design of the triplexer. Figure 6 presents the simulation results of the synthesized triplexer, which exhibits excellent performance in terms of IL, RL, and out-of-band (OoB) rejection.

https://doi.org/10.1017/S175907872610347X Published online by Cambridge University Press

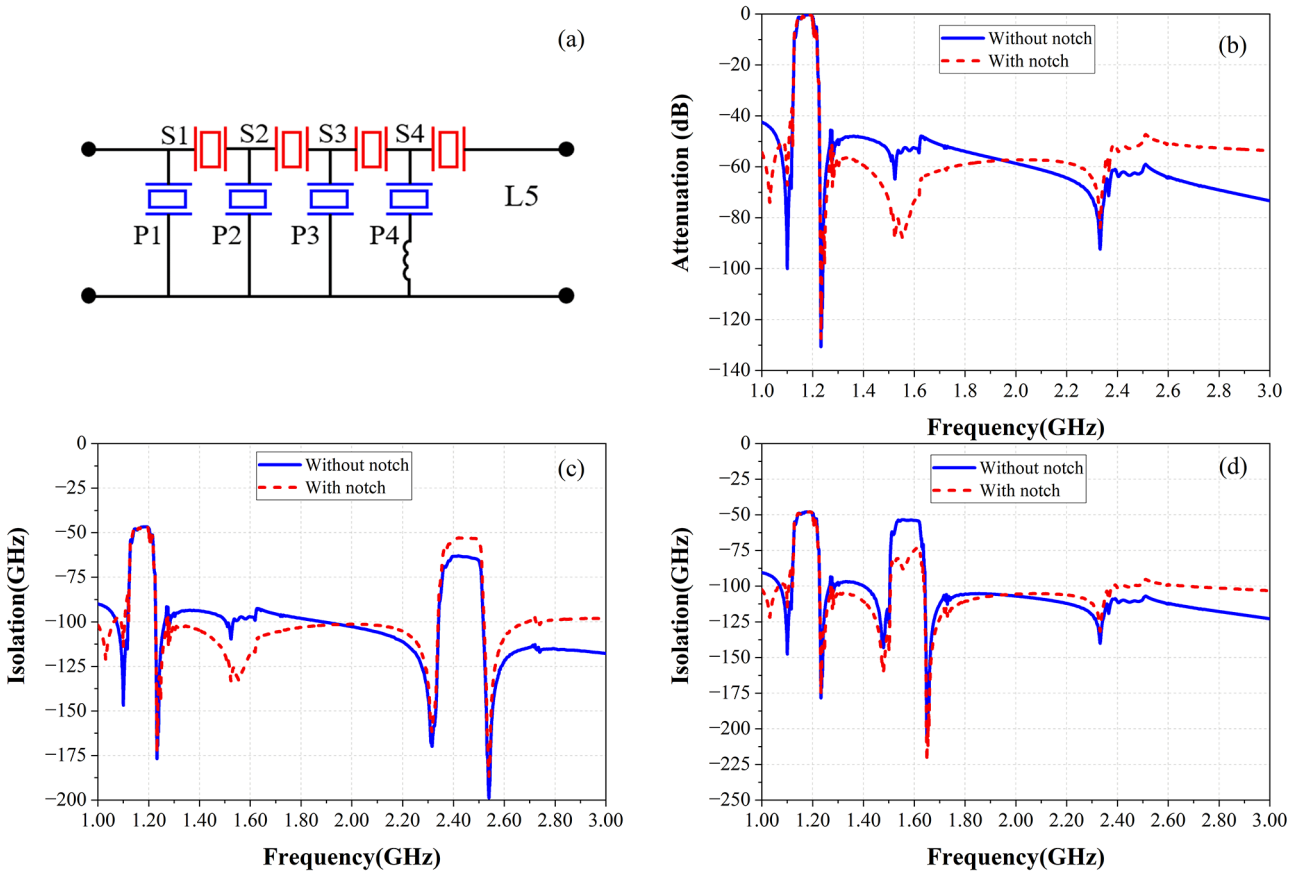


Figure 8. The influence of notch design on triplexer performance. (a) Configuration diagram of the L5 with notch design. (b) The attenuation of the L5 band. (c) The isolation between the L5 and BT bands. (d) The isolation between the L5 and L1 bands.

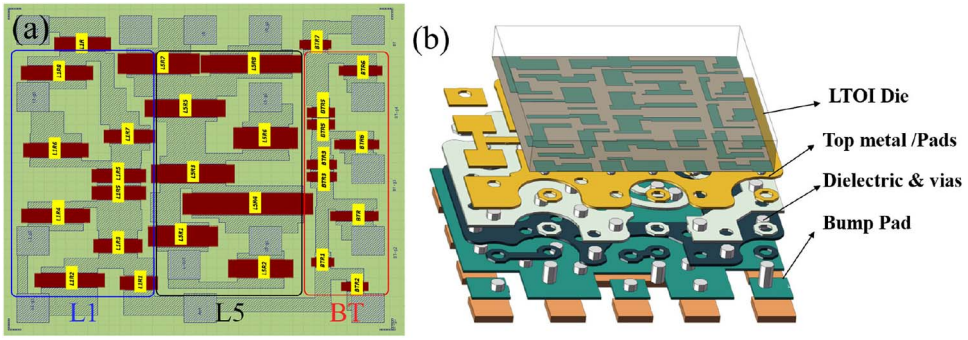


Figure. 9. (a) The layout of the designed triplexer. (b) 3D schematic of the package implementation.

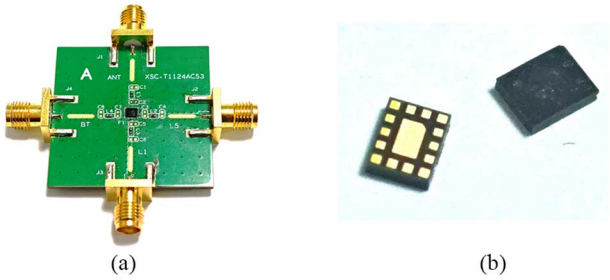


Figure 10. (a) Photograph of the fabricated triplexer mounted on the test board. (b) Photograph of the packaged triplexer.

Isolation improvement of the triplexer

In this work, the three filters are designed based on silicon-based LTOI resonators, which exhibit undesired high-frequency spurious modes at ≈1.4 times the main resonant frequency [28]. The spurious modes arise from the reflection of energy at the silicon substrate. However, this specific spurious mode cannot be simulated by the COM model. Figure 7 shows the admittance response of the typical SAW resonator used in this work. It can be clearly seen that the series resonance frequency of the main resonance mode is about 1.118 GHz, while the series resonance frequency of the high-frequency spurious mode is about 1.574 GHz. This spurious mode forms a small passband, which often affects the out-of-band rejection on the right side of the filter's passband and results in signal leakage.

https://doi.org/10.1017/S175907872610347X Published online by Cambridge University Press

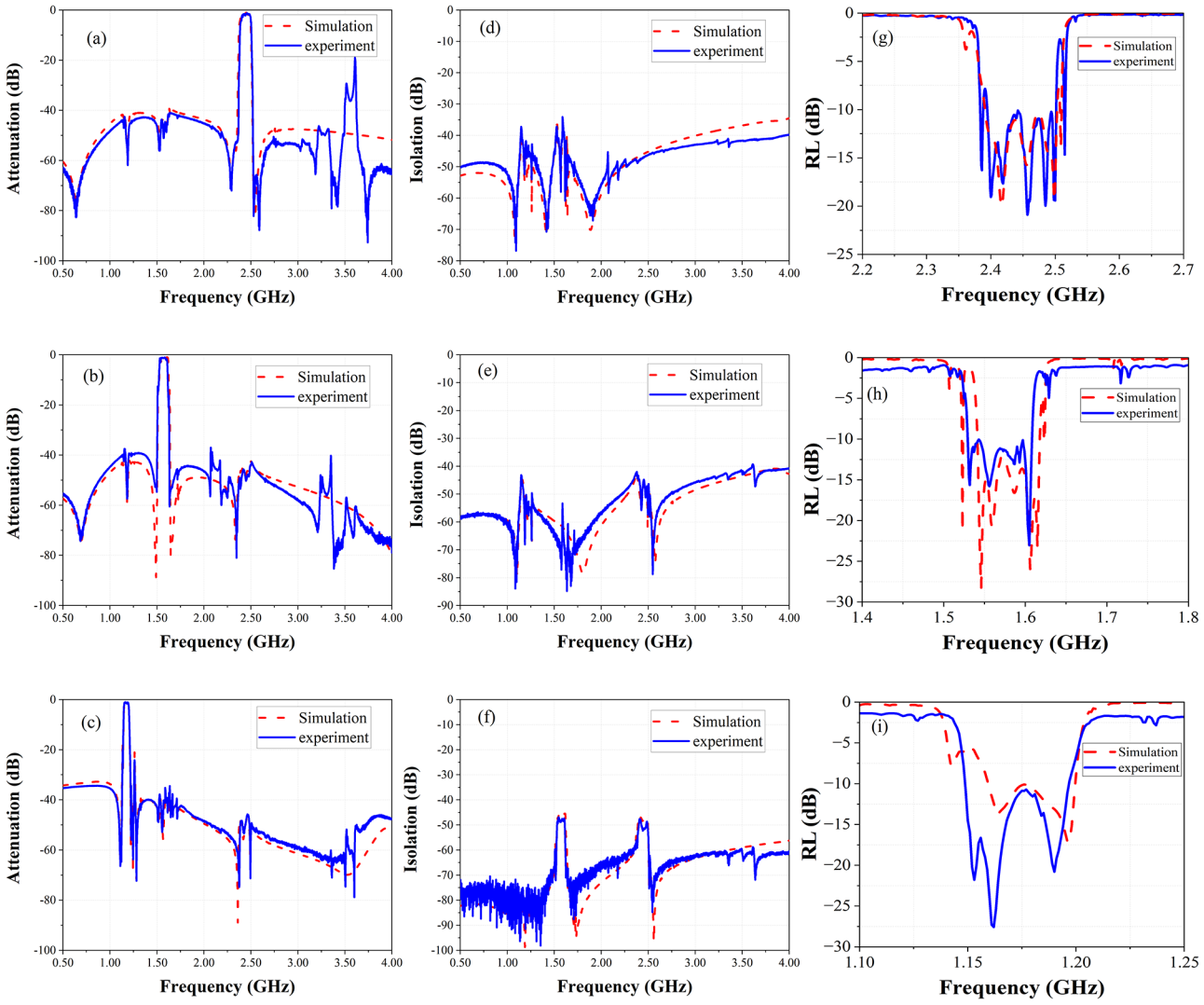


Figure 11. Experimental results and joint simulation results of the triplexer. (a) Response of the BT band. (b) Response of the L1 band. (c) Response of the L5 band. (d) Isolation between the L1 and L5 bands. (e) Isolation between the L5 and BT bands. (f) Isolation between the L1 and BT bands. (g)–(i) present the RL of the fabricated triplexer, respectively.

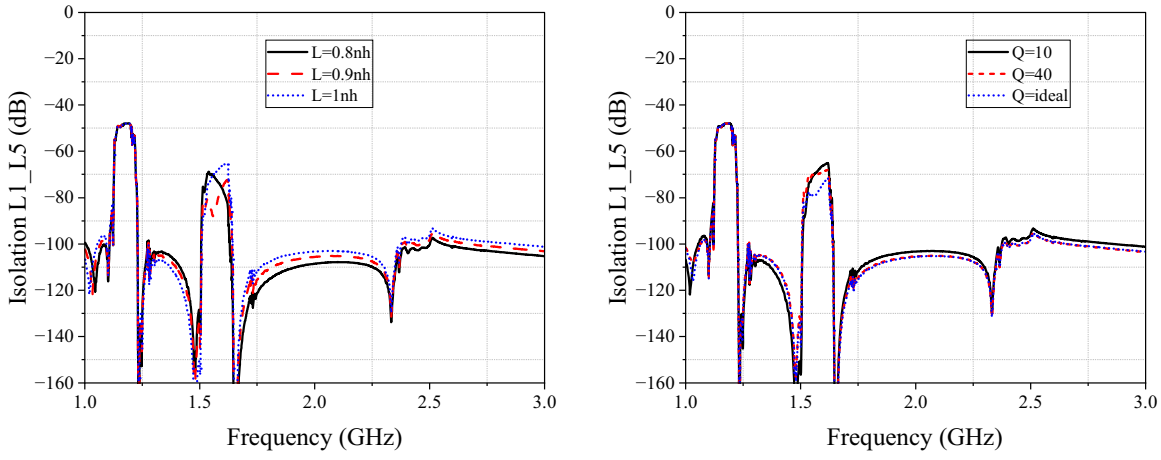


Figure 12. The impact of simulated inductance Q-factor and inductance value on the isolation between the L1 and L5 bands.

https://doi.org/10.1017/S175907872610347X Published online by Cambridge University Press

Table 2. Summary of the measurement results

Section	L5	L1	BT
Freq. (MHz)	1164–1189	1559–1606	2400–2483
IL (dB)	−1.6	−1.6	−2.5 (any 18 MHz)
RL (dB)	−10	−10.16	−11
OoB (dB)	−37	−40	−44
ISO (dB)	L5-BT: −42	L1-BT: −46	L1–L5: −37

In this work, the high-frequency spurious mode of the L5 filter in the triplexer just occurs in the passband of the L1 band. Then, unwanted signal leakage occurs from the L5 filter. At the same time, this also leads to a reduction in isolation between the L5 and L1 bands. Thus, the isolation between the L5 and L1 bands must be improved.

To improve the isolation between adjacent frequency bands caused by high-frequency spurious modes in silicon-based LTOI resonators, as shown in Fig. 8(a), a 0.9-nH inductor is proposed to be added in series with the last grounding elements of the L5 ladder-type filter, thereby introducing a notch in the L1 frequency range. Figure 8(b)–(d) illustrates the responses of the triplexer with a notch. It can be seen from Fig. 8(b) that the attenuation in the L5 band is not affected by the introduction of the inductors. The isolation between the L5 and L1 filters is significantly improved, as shown in Fig. 8(d). Unfortunately, the isolation between the BT and L5 filters degrades as shown in Fig. 8(c). Due to the large margin of isolation between BT/L5 and BT/L1, this degradation is acceptable to a certain extent.

Electromagnetic co-simulation and implementation

In order to ensure better performance, the layout and substrate design of the triplexer were verified through circuit and electromagnetic joint simulations. Figure 9(a) shows the final layout of the triplexer after grounding and routing optimization, with a final size of 1500 μm × 1400 μm. Figure 9(b) shows a 3D view of the triplexer substrate and packaging. The designed organic substrate has a size of 2.5 mm × 2.0 mm, with a dielectric constant of 4.1. A planar spiral inductor is embedded in the substrate to enhance the isolation between the L5 and L1 bands. An impedance matching pad is introduced on the front side of the substrate between the L5 filter and the antenna port.

Device fabrication

The designed triplexer was fabricated and is shown in Fig. 10(b). The filters for the three frequency bands are monolithically integrated on the silicon-based Y-cut 42° LTOI substrate in a monolithic configuration. The device is packaged using Chip Scale Package technology, with a post-packaging size of 2.5 mm × 2.0 mm × 0.6 mm.

Figure 10(a) shows the photograph of the packaged triplexer mounted on the test board for measurement. The antenna port and the three filter ports are connected to SMA connectors through surface-mount coplanar lines. And the electrical performance of the triplexer was measured using a vector network analyzer (Keysight E5071).

Electrical response of the fabricated triplexer

Figure 11 compares the measured performance of the fabricated triplexer with the simulation results. A good agreement is observed between the measurement and the simulation. However, differences are observed near the transmission zeros (TZs) on both sides of the L1 passband, as shown in Fig. 11(b). This could be due to imperfect grounding in the physical circuit, which results in signal leakage. Additionally, the measured triplexer exhibits high-frequency spurious modes on the upper side of each passband, which were not predicted by the COM model used in the design.

The tested triplexer exhibits the expected performance, with IL less than 1.6 dB in the L1 and L5 bands. The maximum IL in the BT band is 3.5 dB, and the average loss within any 18 MHz range of the passband is below 2.5 dB. The RL for all three channels is better than −10 dB. The isolation between the L5 and L1 bands is further improved by embedding a trap inductor within the substrate. However, the isolation does not fully reach the −40 dB target in specific narrow regions of the L1 band. This limitation is likely attributed to the limited Q-factor of the fabricated inductor or a frequency shift of the TZ. As shown in Fig. 12, the inductance Q-factor and inductance value cause a decrease in isolation between L1 and L5. Nevertheless, device performance can be further optimized by enhancing the inductance Q-factor or iteratively adjusting circuit structure parameters.

The detailed measured performance metrics are summarized in Table 2. Table 3 gives a performance comparison of our fabricated triplexer with some reported multiplexers, which shows that the fabricated monolithic integrated triplexer has a compact size, low IL, and high isolation.

Conclusion

In this work, a monolithic integrated triplexer covering the dual-frequency GPS L5/L1 and BT bands is presented. To address the challenge of impedance matching across a wide-bandgap of 1.3 GHz, an analytical synthesis method based on numerical de-embedding was proposed. This method effectively achieves wideband matching without the need for additional matching circuits. Furthermore, considering that high-frequency spurious responses can interfere with other channels in wide-bandgap

Table 3. Performance comparison of reported multiplexers

Ref.	Filter type	Operating frequency (MHz)	Package type	Size (mm × mm)	IL (dB)	RL (dB)	OoB rejection (dB)	Isolation (dB)
[16]	Quadruplexer (SAW)	@2150(B1Rx)	Mutichip	2.65 × 2.15	−5	−12	−43	−50
[13]	Quadruplexer (SAW)	@2350(B40)	Mutichip	3.5 × 3.5	−2.8	−10	−20	\
[15]	Duplexer (SAW)	@2442(WiFi)	Mutichip	\	−3.2	−9	−20	−19
This work	Triplexer	@2442(BT)	Monolithic	2.5 × 2	−2.5	−11	−44	−42

https://doi.org/10.1017/S175907872610347X Published online by Cambridge University Press

triplexer designs, a notch inductor was embedded into the substrate to suppress the specific spurious modes in the upper stopband of the L5 filter. This structure significantly enhances the isolation between the L5 and L1 bands. The designed triplexer is optimized by joint simulation after considering the substrate, layout, and package. The monolithic integrated triplexer realized in this work has a size of 2.5 mm × 2.0 mm × 0.6 mm after packaging, which meets the basic performance requirements for dual-frequency GPS positioning and BT communication applications. The triplexer was successfully fabricated, and experimental characterization demonstrates that the measurement results are in good agreement with the joint simulation data. Monolithic integration offers a promising path to improve chip yield, reduce package size, and reduce parasitic effects. Future work will focus on further enhancing the isolation and overall performance by optimizing the monolithic layout and grounding design. The fabricated triplexer exhibits significant potential for application in increasingly miniaturized RF communication fields, such as wearable devices.

Competing interests. The authors report no conflict of interest.

References

1. **Balteanu F** (2023) Circuits for 5G RF front-end modules. *International Journal of Microwave and Wireless Technologies* **15**, 909–924. https://doi.org/10.1017/S1759078722001295
2. **Fattinger GG, Volatier A, Al-joumayly M, Yusuf Y, Aigner R, Khlat N and Granger-jones M** (2016) Carrier aggregation and its challenges - or: The golden age for acoustic filters. In: *2016 IEEE MTT-S International Microwave Symposium (IMS)*. pp. 1–4. https://doi.org/10.1109/MWSYM.2016.7540211
3. **Detratti M, Lopez E, Perez E, Palacio R and Lobeira M** (2008) Dual-band RF receiver chip-set for Galileo/GPS applications. In *2008 IEEE/ION Position, Location and Navigation Symposium*. Monterey, CA, USA: IEEE, pp. 851–859. https://doi.org/10.1109/PLANS.2008.4569991
4. **Jeon M, Choi WC and Yoon YJ** (2016) GPS, Bluetooth and Wi-Fi tri-band antenna on metal frame of smartwatch In *2016 IEEE International Symposium on Antennas and Propagation (APSURSI)*. Fajardo, PR, USA:IEEE, pp. 2177–2178. https://doi.org/10.1109/APS.2016.7696795
5. **Bouse L, King SA and Chu T** (2024) Simplified indoor localization using Bluetooth beacons and received signal strength fingerprinting with smartwatch. *Sensors* **24**, 2088. https://doi.org/10.3390/s24072088
6. **Ruppel CCW** (2017) Acoustic wave filter technology–A review. *IEEE Transactions on Ultrasonics, Ferroelectrics, and Frequency Control* **64**, 1390–1400. https://doi.org/10.1109/TUFFC.2017.2690905
7. **Chen P, Li G and Zhu Z** (2022) Development and application of SAW filter. *Micromachines* **13**, 656. https://doi.org/10.3390/mi13050656
8. **Takai T, Iwamoto H, Takamine Y, Fuyutsume T, Nakao T, Hiramoto M, Toi T and Koshino M** (2017) I.H.P. SAW technology and its application to microacoustic components (Invited). In *2017 IEEE International Ultrasonics Symposium (IUS)*. Washington, DC, USA: IEEE, pp. 1–8. https://doi.org/10.1109/ULTSYM.2017.8091876
9. **Takai T, Iwamoto H, Takamine Y, Yamazaki H, Fuyutsume T, Kyoya H, Nakao T, Kando H, Hiramoto M, Toi T, Koshino M and Nakajima N** (2017) High-performance SAW Resonator on New Multilayered Substrate Using $LiTaO_3$ Crystal. *IEEE Transactions on Ultrasonics, Ferroelectrics, and Frequency Control* **64**, 1382–1389. https://doi.org/10.1109/TUFFC.2017.2738119
10. **Takamine Y, Takai T, Iwamoto H, Nakao T and Koshino M** (2018) A novel 3.5 GHz low-loss bandpass filter using I.H.P. In *SAW Resonators, in: 2018 Asia-Pacific Microwave Conference (APMC)*. Kyoto: IEEE, pp. 1342–1344. https://doi.org/10.23919/APMC.2018.8617381
11. **Seah X, Ballandras S, Courjon E, Bernard F, Clairet A, Makdissy T, Laroche T, Aspar G, Michoulier E, Ndiaye S, Raveski A, Chappaz C, Hilt T, Alami-idrissi A, Achatz P, Rolland L, Didier C, Allibert F, Drouin A and Huyet I** (2024) High Q-factor low band SAW filter based on high performance POI substrate. In *2024 IEEE MTT-S International Conference on Microwave Acoustics & Mechanics (IC-MAM)*. pp. 125–128. https://doi.org/10.1109/IC-MAM60575.2024.10538490
12. **Yang R-Y, Hsiung C-M, Hung C-Y and Lin -C-C** (2010) Design of a high band isolation Diplexer For GPS and wlan system using modified stepped-impedance resonators. *Progress In Electromagnetics Research* **107**, 101–114. https://doi.org/10.2528/PIER10060913
13. **Jang Y, Ha J-D, Lee S-J, Lim J, Han S-M and Ahn D** (2018) Compact size and wideband triplexer using SAW resonators and LC Components. In *2018 IEEE/MTT-S International Microwave Symposium – IMS*. Philadelphia, PA: IEEE, pp. 856–859. https://doi.org/10.1109/MWSYM.2018.8439454
14. **Yahya SI, Zubir F, Hafez MA, Nkenyereye L, Chaudhary MA, Assaad M, Nouri L, Rezaei A and Jizat NM** (2024) Design and fabrication of a microstrip triplexer with wide flat channels for multi-band 5G applications. *PLoS One* **19**, e0302634. https://doi.org/10.1371/journal.pone.0302634
15. **Yang M-Y and Wu R-B** (2023) Design for SAW antenna-plexers with improved matching inductance circuits. *Micromachines* **15**, 89. https://doi.org/10.3390/mi15010089
16. **Tseng S-Y, Yang M-Y, Hsiao -C-C, Chen -Y-Y and Wu R-B** (2022) Design for acoustic wave multiplexers with single inductor matching network using frequency response fitting method. *IEEE Open Journal of Ultrasonics, Ferroelectrics, and Frequency Control* **2**, 140–151. https://doi.org/10.1109/OJUFFC.2022.3182321
17. **Liu X, Pei W, Zhao J, Xu R, Zhong Y and Yu D** (2025) A review of wafer-level packaging technology for SAW and BAW filters. *Micromachines* **16**, 320. https://doi.org/10.3390/mi16030320
18. **Joseph SD and Ball EA** (2025) Analysis of bondwires and RF compensation circuits in E-band. *IEEE Transactions on Components, Packaging and Manufacturing Technology* **15**, 1986–1995. https://doi.org/10.1109/TCPMT.2025.3594505
19. **Iwaki M, Tanaka T, Ueda M and Satoh Y** (2017) Design consideration on converged Rx SAW duplexer module for multiband RF front end. *IEEE Transactions on Microwave Theory & Techniques* **65**, 4629–4635. https://doi.org/10.1109/TMTT.2017.2742955
20. **Volatier A, Fattinger G, Dumont F, Stoyanov P and Aigner R** (2013) Technology enhancements for high performance BAW duplexer. In *2013 IEEE International Ultrasonics Symposium (IUS)*. Prague, Czech Republic: IEEE, pp. 761–764. https://doi.org/10.1109/ULTSYM.2013.0196
21. **Iwaki M, Tsutsumi J, Tanaka T, Ueda M and Satoh Y** (2014) A converged Rx SAW duplexer module with embedded substrate for multi-band RF front-end. In *2014 IEEE MTT-S International Microwave Symposium (IMS2014)*. Tampa, FL, USA: IEEE, pp. 1–3. https://doi.org/10.1109/MWSYM.2014.6848617
22. **Song K, Luo M, Zhong C, Chen Y, Zhou Y and Xia F** (2021) Compact multimode-resonator multiplexer with wide upper-stopband and high isolation. *International Journal of Microwave and Wireless Technologies* **13**, 111–118. https://doi.org/10.1017/S1759078720001063
23. **Moloudian G and Dousti M** (2018) Design and fabrication of a compact microstrip lowpass-bandpass diplexer with high isolation for telecommunication applications. *International Journal of RF and Microwave Computer-Aided Engineering* **28**, e21248. https://doi.org/10.1002/mmce.21248
24. **Rezaei A and Noori L** (2018) Novel compact microstrip diplexer for GSM applications. *International Journal of Microwave and Wireless Technologies* **10**, 313–317. https://doi.org/10.1017/S1759078718000168
25. **Silveira P, Verdú J and De Paco P** (2020) Scattering matrix solution for an ideal star-junction multiplexer based on ladder-type filters. *International Journal of Microwave and Wireless Technologies* **12**, 954–959. https://doi.org/10.1017/S1759078720000422
26. **Takai T, Iwamoto H, Takamine Y, Wada T, Hiramoto M, Koshino M and Nakajima N** (2016) Investigations on design technologies for SAW quadplexer with narrow duplex gap. In *2016 IEEE MTT-S International*

Microwave Symposium (IMS). San Francisco, CA: IEEE, pp. 1–4. https://doi.org/10.1109/MWSYM.2016.7540214

27. **Hashimoto K** (2000) *Surface Acoustic Wave Devices in Telecommunications*. Berlin Heidelberg: Springer. https://doi.org/10.1007/978-3-662-04223-6
28. **Inoue S and Solal M** (2018) Spurious free SAW resonators on layered substrate with ultra-high Q, high coupling and small TCF. In *2018 IEEE International Ultrasonics Symposium (IUS)*. Kobe, Japan: IEEE, pp. 1–9. https://doi.org/10.1109/ULTSYM.2018.8579852

Appendix

The IDT parameters of the triplexer resonator are shown in Table A1.

Table A1. IDT parameters of the SAW resonators used in the triplexer

Filter-resonator	*P* (μm)	*W*	*N*
L5-Series-1	1.658	45P	58
L5-Parallel-1	1.746	55P	105
L5-Series-2	1.660	45P	67
L5-parallel-2	1.757	55P	105
L5-Series-3	1.651	45P	81
L5-parallel-3	1.761	55P	102
L5-Series-4	1.654	45P	54
L5-Parallel-4	1.753	55P	103
L1-Series-1	1.217	55P	60
L1-Parallel-1	1.281	45P	120
L1-Series-2	1.212	45P	89
L1-Parallel-2	1.284	45P	96
L1-Series-3	1.217	45P	87
L1-Parallel-3	1.287	45P	117
L1-Series-4	1.215	45P	76
L1-Parallel-4	1.283	52P	108
L1-Series-5	1.218	51P	88
BT-Series-1	0.762	45P	50
BT-Parallel-1	0.8	45P	102
BT-Series-2	0.764	45P	52
BT-Parallel-2	0.807	48P	131
BT-Series-3	0.762	45P	50
BT-Parallel-3	0.806	45P	119
BT-Series-4	0.762	45P	85
BT-Parallel-4	0.801	48P	149

P = half period of IDT; *N* = number of IDT pairs, *W* = aperture.



Peiran Li received his M.E. degree in Electronic Communication Engineering from the University of Electronic Science and Technology of China (UESTC), Chengdu, China, in 2021. He is currently pursuing his Ph.D. degree in Integrated Circuit Science and Engineering at UESTC. His current research interests include the design and simulation of surface and bulk acoustic wave devices, research on Lamb wave modes in surface acoustic wave resonators, and the finite-element method (FEM) simulation method.



Bin Peng received the Ph.D. degree in microelectronics from the University of Electronic Science and Technology of China, Chengdu, China, in 2008. He is currently a professor with the University of Electronic Science and Technology of China, and has deep attainments in acoustics and electromagnetics. His current research mainly focuses on surface acoustic wave devices technology.



Zijie Wei received the M.Sc. degree in materials science and engineering from the University of Electronic Science and Technology of China, Chengdu, China, in 2021. He is currently pursuing the Ph.D. degree in electronic science and technology with the National Key Lab of Electronic Thin Films and Integrated Devices, University of Electronic Science and Technology of China, Chengdu, China. His current research field is the fabrication of single-crystal thin film devices.



Wei Fan was born in Changchun, China, in 1995. He received the B.S. degree in physics from Jilin University, Changchun, China, in 2018. He received the M.S. degree in electronic science and technology from the University of Electronic Science and Technology of China (UESTC), Chengdu, China, in 2023, where he is currently pursuing the Ph.D. degree in Integrated Circuit Science and Engineering at the School of Integrated Circuit Science and Engineering. His research interests include the design and simulation of high-frequency surface acoustic wave (SAW) resonators and filters, and the suppression method of transverse modes of S0 mode SAW resonators.

https://doi.org/10.1017/S175907872610347X Published online by Cambridge University Press



Yuedong Wang received the bachelor's degree in microelectronics science and engineering from the University of Electronic Science and Technology of China, Chengdu, China, in 2017. He is currently pursuing the Ph.D. degree in electronic science and technology with the National Key Lab of Electronic Thin Films and Integrated Devices, University of Electronic Science and Technology of China, Chengdu, China. His current research field is the design and fabrication of single-crystal thin film devices.



Dahao Wu was born in Shanxi, China, in 1999. He received the B.Eng. and master's degrees from the University of Electronic Science and Technology of China (UESTC), Chengdu, China, in 2021 and 2024, respectively. He is currently pursuing the Ph.D. degree at the School of Integrated Circuit Science and Engineering, under the supervision of Prof. Chuangui Wu and Prof. Yao Shuai. His current research interests include the simulation and design of surface and bulk acoustic wave devices, and the finite-element method (FEM) simulation method.



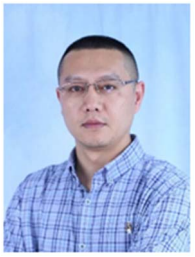
Lu Lv received his bachelor's degree from Tianjin University in 2014 and his doctorate from the University of Electronic Science and Technology of China in 2023. Currently, he is working at the 29th Research Institute of China Electronics Technology Group Corporation. His current research interests are related to acoustics and RF components.



Wenbo Luo received the B.S. degree in electronic science and technology and the Ph.D. degree in material physics and chemistry from the University of Electronic Science and Technology of China, Chengdu, China, in 2004 and 2010, respectively. He is currently working as a Professor with the State Key Laboratory of Electronic Thin Films and Integrated Devices, University of Electronic Science and Technology of China. His current research fields are growth and characterization of oxide function films.



Xinqiang Pan received the B.S. degree in electronic science and technology from the University of Electronic Science and Technology of China in 2013, and the Ph.D. degree in Micro-Electronics and Solid-State Electronics from the University of Electronic Science and Technology of China in 2019. He worked as a postdoctoral researcher at the University of Electronic Science and Technology of China from 2020 to 2022. He currently works as an associate professor at the University of Electronic Science and Technology of China. His current research interests include electronic thin films and electronic device (such as filter, memristor, etc.).



Yao Shuai received the Ph.D. degree in physics from the Technical University of Dresden, Dresden, Germany, in 2013. He is a professor at the School of Integrated Circuit Science and Engineering, University of Electronic Science and Technology of China (UESTC), Chengdu, China. His current research interests include the fabrication of functional oxide thin films, surface acoustic waves, and bulk acoustic wave devices.



Chuangui Wu received the B.Sc. degree in electronic materials and devices, the M.Sc. degree, and the Ph.D. degree in material physics and chemistry from the University of Electronic Science and Technology of China (UESTC), Chengdu, China, in 2001, 2004, and 2009, respectively. He is currently a professor with the National Key Laboratory of Electronic Thin Films and Integrated Devices, UESTC. His current research interests include electronic thin films and integrated devices.

https://doi.org/10.1017/S175907872610347X Published online by Cambridge University Press